第 33 卷第 9 期
2017 年 9 月

无 机 化 学 学 报
CHINESE JOURNAL OF INORGANIC CHEMISTRY

Vol.33 No.9
1656-1666

Bi_2WO_6/TiO_2 纳米管异质结构复合材料的多模式下的光催化活性比较

马凤延*,[1] 杨 阳[1] 李 娜[1] 杨麒麟[1] 李尚锦[2] 申路严[2]

([1] 齐齐哈尔大学化学与化学工程学院,齐齐哈尔 161006)

([2] 齐齐哈尔大学材料科学与工程学院,齐齐哈尔 161006)

摘要:以 TiO_2 纳米管为模板,采用多组分自组装结合水热法制备 Bi_2WO_6/TiO_2 纳米管异质结构复合材料。通过多种技术如 X 射线衍射(XRD),X 射线光电子能谱(XPS),N_2 吸附-脱附,扫描电镜(SEM),高分辨透射电镜(HRTEM)和紫外可见漫反射吸收光谱(UV-Vis DRS)考察所制备样品的组成、结构、形貌、光吸收和电子性质。Bi_2WO_6 纳米片或纳米粒子分布在 TiO_2 纳米管上,形成异质结构。随后,通过在紫外、可见和微波辅助光催化模式下降解染料罗丹明 B(RhB)来评价复合催化剂的光催化活性。与 TiO_2 纳米管和 Bi_2WO_6 相比,Bi_2WO_6/TiO_2-35 纳米管在多模式下表现出更优异的光催化活性。与紫外和可见降解模式相比,Bi_2WO_6/TiO_2-35 纳米管在微波辅助光催化模式下对 RhB 的降解效率最高。这种增强的光催化活性源于适量 Bi_2WO_6 的引入、纳米管独特的形貌特征和降解模式所引起的增强的量子效率。降解过程中的活性物种被证明是 h^+,·OH 和 $\cdot O_2^-$自由基。而且,在微波辅助光催化模式下,可产生更多的·OH 和 $\cdot O_2^-$自由基。

关键词:TiO_2 纳米管;Bi_2WO_6;多模式降解;光催化

中图分类号:TB33 **文献标识码**:A **文章编号**:1001-4861(2017)09-1656-11

DOI:10.11862/CJIC.2017.199

Comparison of Photocatalytic Activity of Bi_2WO_6/TiO_2 Nanotubes Heterostructures Composite under Multimode

MA Feng-Yan*,[1] YANG Yang[1] LI Na[1] YANG Qi-Lin[1] LI Shang-Jin[2] SHEN Lu-Yan[2]

([1]*College of Chemistry and Chemical Engineering, Qiqihar University, Qiqihar, Heilongjiang* 161006, *China*)

([2]*College of Materials Science and Engineering, Qiqihar University, Qiqihar, Heilongjiang* 161006, *China*)

Abstract: Bi_2WO_6/TiO_2 nanotubes (Bi_2WO_6/TiO_2-NTs) heterostructures composite were synthesized by multicomponent assembly approach combined with hydrothermal treatment employed TiO_2 nanotubes as template. Multiple techniques such as X-ray powder diffraction (XRD), X-ray photo-electron spectroscopy (XPS), N_2 adsorption-desorption, scanning electron microscopy (SEM), high resolution transmission electron microscopy (HRTEM), and UV-Vis diffused absorption spectra (UV-Vis DRS) were applied to investigate the composition, structures, morphologies, optical and electronic properties of as-prepared samples. The heterostructures were formed with Bi_2WO_6 nanoflakes or nanoparticles attached on the surface of TiO_2 nanotubes. The photocatalytic activity of Bi_2WO_6/TiO_2-NTs heterostructures was evaluated sufficiently by photodegradation of rhodamine B (RhB) under multimode including UV, visible and microwave-assisted photocatalysis. Compared to TiO_2 nanotubes and Bi_2WO_6, Bi_2WO_6/TiO_2-NTs-35 shows the highest photocatalytic activity under multimode. In contrast with UV, visible mode, the Bi_2WO_6/TiO_2-NTs-35 shows the highest activity toward RhB degradation under microwave-assisted photocatalytic mode. This enhanced photocatalytic activity is due to the more efficient separation of the

收稿日期:2017-04-18。收修改稿日期:2017-07-18。

国家自然科学基金(No.21376126,81403067)、齐齐哈尔大学青年教师科学技术类科研启动支持计划项目(No.2014K-M03)和黑龙江省教育厅基本业务专项理工面上项目(No.135109204)资助。

*通信联系人。E-mail:mafengyan989@163.com

e^--h^+ pairs, originating from the introduction of Bi_2WO_6 modified TiO_2-NTs, the nanotubular geometries, and degradation mode. The main active species of the degradation process are proven to be h^+, ·OH, and $\cdot O_2^-$ radicals. Moreover, more ·OH and $\cdot O_2^-$ radicals were generated under microwave-assisted photocatalytic mode.

Keywords: TiO_2 nanotubes; Bi_2WO_6; multimode degradation; photocatalysis

0 Introduction

Titanium dioxide (TiO_2) has attracted a great deal of research attention because of their potential applications in the photodegradation of organic pollutants, photocatalytic water splitting for hydrogen generation, dye-sensitized solar cells, and even gas sensors and biosensors, due to its low cost and abundant elements (Ti and O), long-term stability, and environmental-friendly characteristics[1-3]. However, its wide band gap and fast recombination of the photogenerated electron-hole (e^--h^+) are two limitations for its contemporary applications[4].

To overcome the above limitations, some measures have been taken. At present, one effective approach is to adjust TiO_2 morphology. One-dimensional (1D) TiO_2 nanomaterials have been receiving extensive interests[5-8]. Moreover, compared with other forms of TiO_2, titania nanotubes possess the distinguishing features of nanotubes including large specific surface area, good electron/proton conductivity, and high aspect ratio. In addition, the open mesoporous morphology of TiO_2 nanotubes can efficiently transfer the electrons along the 1D path without grain boundaries and junctions, while hollow space can capture scattered light to increase light harvesting as well as easier separation and recovery than TiO_2 nanoparticles due to the length in the micrometer range[9].

Another strategy is to construct the heterostructures by the wide band-gap semiconductor with a narrow band-gap semiconductor (with the proper band positions)[1,10]. Yu and Li fabricated and reported Ag-based heterojunction[11-16], Au NPs loaded onto the α-$Bi_2O_3/Bi_2O_2CO_3$[17], F-Bi_2MoO_6[18], anatase/rutile TiO_2 particles[19], and MoS_2/CdS composite[20], which are more efficient than individual component in photocatalytic properties. In particular, Qian and Ma groups successfully fabricated UCNPs/semiconductors for NIR-driven photocatalysis, such as UCNPs/TiO_2 nanofiber[21], UCNPs/TiO_2/CdS nanofibers[22], NYF@TiO_2-Au core@shell microspheres[23]. They show unique optical properties with wide absorption and enhanced photocatalytic abilities towards to organic dye removal efficiency under irradiation with NIR. Such synergistic interactions of heterojunction between two kinds of semiconductors are fairly powerful not only in improving the visible light harvesting ability but also in extending the lifetime of photoinduced electrons and holes via an internal charge transfer, facilitating the separation of electron-hole pairs and reducing the chance of recombination[24-26].

Among these, bismuth tungstate (Bi_2WO_6), as a typical Aurivillius oxide, has a layered structure with perovskite-like slabs of WO_6 and $[Bi_2O_2]^{2+}$ layer and has important physical and chemical properties such as ferroelectric piezoelectricity, catalytic behavior and nonlinear dielectric susceptibility[27-28]. More importantly, Bi_2WO_6 is a promising visible light-driven photocatalyst with high photocatalytic activity[29-30]. However, the photocatalytic activity of pure Bi_2WO_6 is limited by difficult migration and high recombination probability of photogenerated e^--h^+ pairs. Therefore, the combination of tubular morphology and heterostructure construction is a useful approach for designing heterostructure photocatalysts with high charge separation efficiency.

In order to improve the photocatalytic activity, the construction of TiO_2-Bi_2WO_6 heterostructures has become a hot research, and some achievement has been obtained in recent years. For instance, Wang et al. successfully synthesized TiO_2-Bi_2WO_6 nanofibers by electrospinning technique[31]. Colón et al. and other groups have reported TiO_2 modified flower[32]/sphere[33]/hollow tube-like Bi_2WO_6 [34]. Wu and Luo et al. reported the preparation TiO_2 nanobelts[35]/TiO_2 nanotubes[36]

grown on titanium (Ti) foil decorated with Bi_2WO_6 nanocrystals, respectively. These results indicate that the photocatalytic activities of TiO_2-Bi_2WO_6 heterojunctions show enhanced photocatalytic performance in comparison with individual components of Bi_2WO_6 or TiO_2. To the best of our knowledge, much less notice has been taken of the preparation of TiO_2 nanotubes synthesized by alkali hydrothermal treatment modified with Bi_2WO_6. Moreover, few investigations were carried on the comparative mechanism of the enhanced photocatalytic activity for organic pollutants under multiple modes including UV, visible, and microwave-assisted photocatalysis. What is more, they lack direct evidence to explain photocatalytic mechanism under multiple modes that serve as background data for the environmental behavior of organic pollutants.

In this work, Bi_2WO_6/TiO_2 nanotubes (Bi_2WO_6/TiO_2-NTs) heterostructures were fabricated by multicomponent assembly approach combined with hydrothermal treatment, which is free from the usage of additives or surfactants. Subsequently, the photocatalytic activities of Bi_2WO_6/TiO_2 nanotubes under multiple modes including UV, visible, and microwave-assisted photocatalysis were also studied in this work. Direct evidence to explain comparatively photocatalytic mechanism under multiple modes was supplied by free radical and hole trapping experiments. The relationship between the morphology, structure, optical properties and the photocatalytic activities of Bi_2WO_6/TiO_2 heterostructures under multiple modes was investigated in detail.

1 Experimental

1.1 Preparation of Bi_2WO_6/TiO_2 nanotubes

In a typical procedure[37], TiO_2 nanotubes were dispersed in H_2O (5 mL) under vigorously stirring for 0.5 h. Meanwhile, $Bi(NO_3)_3 \cdot 5H_2O$ (0.972 g) and $Na_2WO_4 \cdot 2H_2O$ (0.329 g) were dissolved in glacial acetic acid (HAc, 10 mL) and H_2O (5 mL), respectively. Subsequently, the above solutions were added into TiO_2 nanotubes suspension to form a white suspension. After stirring for 2 h, the resulting mixture was suffered from hydrothermal treatment at 150 ℃ for 4 h, and the resulting precipitate was dried and washed with deionized water for three times. The obtained powder was further dried at 80 ℃ for 24 h. The final product was denoted as Bi_2WO_6/TiO_2-NTs-x, where x represents the doping of TiO_2 nanotubes (mass percentage).

1.2 Characterization of the catalyst

X-ray diffraction patterns were obtained on a Bruker-AXS (D8) X-ray diffractometer with Cu $K\alpha$ radiation (λ=0.154 06 nm) at 40 kV and 40 mA in 2θ ranging from 20° to 80°. X-ray photoelectron spectroscopy (XPS) characterization was carried out on an ESCALAB 250Xi spectrometer equipped with Al $K\alpha$ radiation at 300 W. N_2 adsorption-desorption isotherm analyses of samples were obtained at 77 K using Micromeritics 3H-2000PS2. The morphologies of synthesized samples were analyzed using a scanning electron microscope (SEM) (HitachiS-4300) and transmission electron microscope (TEM) and high resolution transmission electron microscope (HRTEM) (JEM-2100F). UV-Vis diffused absorption spectra (UV-Vis DRS) were recorded using a UV-Vis spectrophotometer (TU-1901) over the wavelength range of 200~800 nm and $BaSO_4$ as a reference material.

1.3 Photocatalytic tests

Photocatalytic activities of the Bi_2WO_6/TiO_2-NTs composite were studied by monitoring the degradation behaviors of rhodamine B (RhB) under multimode (including UV, visible, and microwave-assisted photocatalysis mode). The 125 W high pressure mercury lamp (λ=313.2 nm), 400 W Xe lamp (λ=410.0 nm; moreover, the inner sleeve was made of No. 11 glass to filter out ultraviolet from the Xe lamp), and 15 W microwave electrodeless lamp (MEL, UV emission wavelength mainly located at 278 nm, U shape, 100 W output power of microwave reactor), were used as UV, visible light, and microwave-assisted photocatalysis mode light source, respectively. The concetration of RhB was 50 $mg \cdot L^{-1}$. Moreover, the amounts of the catalyst (liquid volume) for the three modes (UV, visible, and microwave-assisted photocatalysis) were 100 mg (100 mL), 200 mg (220 mL), and 300 mg

(500 mL), respectively.

The photocatalytic reaction was carried out in a quartz photoreactor. Prior to irradiation, the suspension containing the solid catalyst and an aqueous solution of the contaminant was ultrasonicated for 10 min and then stirred for 1.5 h in the dark to ensure adsorption-desorption equilibrium. The reaction temperature was maintained at (30±2) ℃ by circulation of water through an external cooling jacket or by circulating solution to a cooler with the peristaltic pump. At certain time intervals, suspensions (5 mL) were sampled and centrifuged to remove the photocatalyst particles. Decreases in the concentrations of RhB, methyl orange (MO), crystal violet (CV), and methylene blue (MB) were analyzed by TU-1901 UV-Vis spectrophotometer at λ=553, 464, 582, and 664 nm, respectively.

2 Results and discussion

2.1 Compositional and structural information

XRD was used to characterize the crystal structure of the as-prepared Bi_2WO_6/TiO_2-NTs, as well as pure TiO_2-NTs and Bi_2WO_6 (Fig.1). The diffraction peaks of pure TiO_2-NTs and Bi_2WO_6 are well matched with the standard patterns of anatase phase of TiO_2 (PDF No.21-1272) [37] and orthorhombic phase of Bi_2WO_6 (PDF No.39-0256), respectively. After the coupling of Bi_2WO_6 and TiO_2-NTs, when the TiO_2-NTs loading increases from 25% to 50%, the diffraction peaks of TiO_2 intensify gradually, whereas the peak intensities of Bi_2WO_6 decrease. No impurity peak is found in Bi_2WO_6/TiO_2-NTs composites, suggesting that the composites exhibit a coexistence of both Bi_2WO_6 and TiO_2 phases.

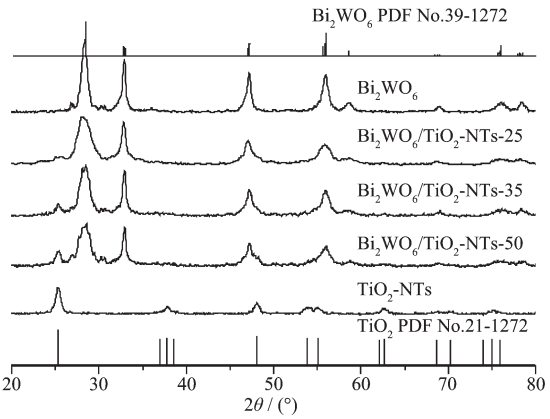

Fig.1　XRD patterns of the samples

Valence states and the surface chemical composition of the as-prepared samples were investigated by XPS technique. As shown in Fig.2a, the peaks at 458.68 and 464.48 eV are attributed to Ti2$p_{3/2}$ and Ti2$p_{1/2}$, respectively, confirming the titanium species in the composite is Ti^{4+}. After introduction of the Bi_2WO_6 into the TiO_2 nanotubes, the binding energies of Ti2$p_{3/2}$ and Ti2$p_{1/2}$ shift to higher values (458.78 and 465.28 eV, respectively), which is attributed to diffusion of W^{6+} ions into the TiO_2 lattice and further generation of WOTi bond linkage[35,37]. As displayed in Fig.2b and c, for pure Bi_2WO_6, the characteristic peaks at 164.58 and 159.28 eV are ascribed to Bi4$f_{5/2}$ and Bi4$f_{7/2}$ from Bi^{3+} in the lattice and the binding energy of W4$f_{5/2}$ and W4$f_{7/2}$ at 37.88 and 35.78 eV, respectively, are corresponded to W^{6+} [35]. In the XPS spectrum of Bi_2WO_6/TiO_2-NTs, in contrast with Bi_2WO_6, the binding energy of Bi4$f_{5/2}$ (164.38 eV) and Bi4$f_{7/2}$ (159.08 eV) decreases by 0.2 eV while that of W4$f_{5/2}$ (37.58 eV)and W4$f_{7/2}$ (35.58 eV) decreases by 0.3 eV. The results suggest that the chemical environment surrounding Bi and W has changed, which is possibly

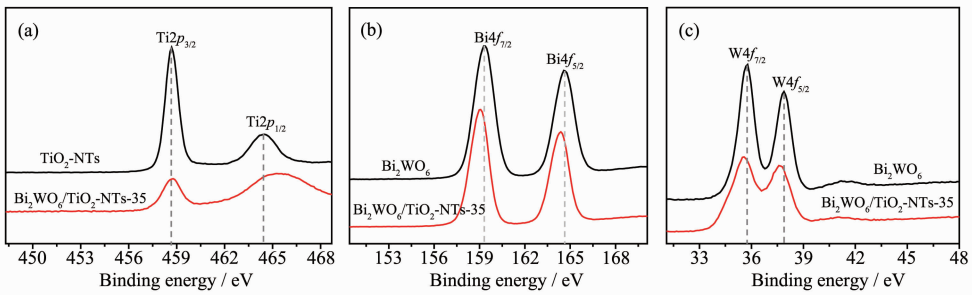

Fig.2　XPS spectra of Ti2p (a), Bi4f (b), and W4f (c) regions for TiO_2-NTs, Bi_2WO_6, and Bi_2WO_6/TiO_2-NTs-35

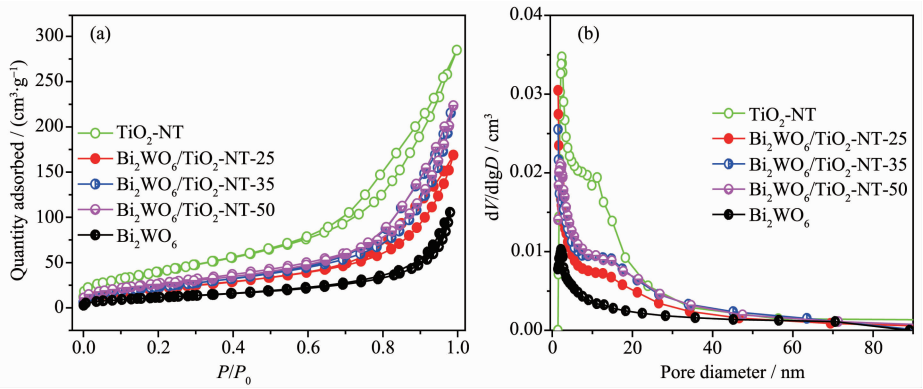

Fig.3 Nitrogen adsorption-desorption isotherms (a) and BJH pore size distribution curves (b) of samples

Table 1 Textural parameters of various TiO_2-based materials

Sample	S_{BET} / ($m^2 \cdot g^{-1}$)	V_p / ($cm^3 \cdot g^{-1}$)	D_p / nm
TiO_2-NTs	151	0.44	8.50
Bi_2WO_6	44	0.16	10.44
Bi_2WO_6/TiO_2-NTs-25	80	0.26	9.12
Bi_2WO_6/TiO_2-NTs-35	88	0.33	10.20
Bi_2WO_6/TiO_2-NTs-50	101	0.35	9.84

influenced by TiO_2-NTs. Thus, we can confirm that the TiO_2-NTs successfully modified by Bi_2WO_6.

The porosity of the Bi_2WO_6/TiO_2-NTs heterostructures is investigated by N_2 adsorption-desorption isotherms and the corresponding BJH pore size distribution. As shown in Fig.3a, the isotherms exhibit type Ⅳ with an H3 hysteresis loop characteristic of mesoporous material[37], which is confirmed by the pore size distribution (Fig.3b). Moreover, the formation of such mesoporous materials is attributed to the aggregation of the Bi_2WO_6 nanoparticles adhering to the surface of the TiO_2 nanotubes. More importantly, as shown in Table 1, the measured BET surface areas of Bi_2WO_6/TiO_2-NTs-25 (80 $m^2 \cdot g^{-1}$), Bi_2WO_6/TiO_2-NTs-35 (88 $m^2 \cdot g^{-1}$) and Bi_2WO_6/TiO_2-NTs-50 (101 $m^2 \cdot g^{-1}$) are greatly enhanced compared with that of Bi_2WO_6 (44 $m^2 \cdot g^{-1}$). Meanwhile, the specific surface areas of composite materials increase indeed together with the increase of TiO_2-NTs contents from 25% to 50%.

2.2 Morphology

The morphology and microstructure of the photocatalysts were also investigated. As shown in the SEM image (Fig.4a), TiO_2-NTs show the nanotubular morphology with an average diameter of 30 nm and

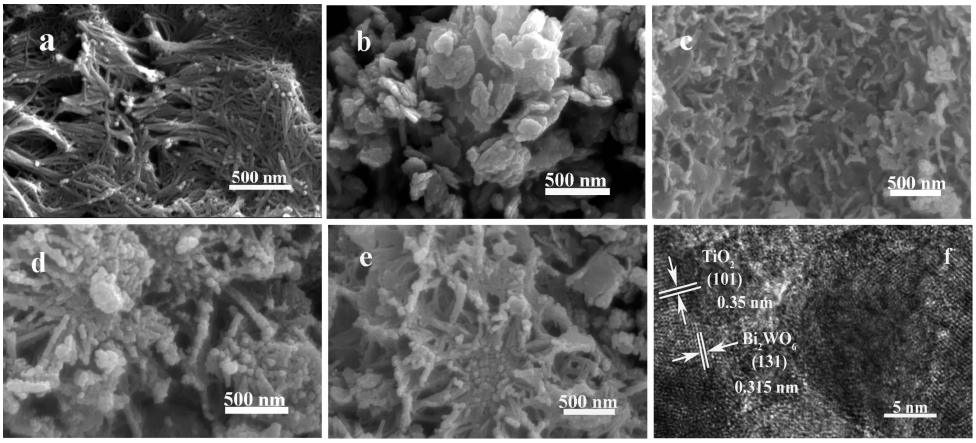

(a) TiO_2-NTs, (b) Bi_2WO_6, (c) Bi_2WO_6/TiO_2-NTs-25, (d) Bi_2WO_6/TiO_2-NTs-35, (e) Bi_2WO_6/TiO_2-NTs-50, (f) HRTEM image of Bi_2WO_6/TiO_2-NTs-35

Fig.4 SEM images of the samples

length of 1 μm. While Bi_2WO_6 exhibits a typical structure of nanosheet consist of nanoparticles with the side length of 50~250 nm and thickness of 20~40 nm (Fig.4b). As displayed in Fig.4c~e, morphologies of TiO_2 and Bi_2WO_6 change obviously after the combination by TiO_2-NTs and Bi_2WO_6 through hydrothermal treatment. The typical morphology structure of Bi_2WO_6/TiO_2-NTs-25 consists of smooth TiO_2 nanotubes and curled Bi_2WO_6 flakes, which link mutually to each other. Moreover, the surface of TiO_2 nanotubes becomes rough obviously after Bi_2WO_6 modification when TiO_2 nanotubes loading increases from 35% to 50%. While Bi_2WO_6 changes from flakes to smaller nanoparticles. Furthermore, smaller Bi_2WO_6 nanoparticles homogeneously disperse on the surface of TiO_2 nanotubes *in-situ* growth process. Compared with TiO_2 -NTs and Bi_2WO_6, aggregation of Bi_2WO_6/TiO_2-NTs has intensively alleviated with the loading of TiO_2 nanotubes increasing from 0 to 50%.

In order to further confirm the Bi_2WO_6/TiO_2-NTs heterostructures, HRTEM was used to investigate the detailed structure information of the Bi_2WO_6/TiO_2-NTs. The corresponding HRTEM image displays two types of clear lattice fringes, as shown in Fig.4f. The interplanar spacing of 0.35 and 0.315 nm corresponds to the (101) crystal plane of TiO_2-NTs and the (131) crystal plane of the orthorhombic phase of Bi_2WO_6, respectively[18-19]. According to the results of XRD, XPS, SEM and HRTEM, we assume that Bi_2WO_6/TiO_2-NTs heterostructures with Bi_2WO_6 nanoparticles on the surface of TiO_2 nanotubes have been prepared successfully.

Based on the above results and discussion, we put forward the plausible formation of Bi_2WO_6/TiO_2-NTs heterojunction. Considering $Bi(NO_3)_3$ with crystal water, $Bi_2O_2(OH)NO_3$ is formed through the following hydrolysis and condensation reaction in the glacial acetic acid-water system (Eq.**1** ~**2**). When Na_2WO_4 solution is added to the above reaction solution, Bi_2WO_6 nanoparticles are obtained (Eq.**3**)[38]. Then the introduction of TiO_2-NTs into Bi_2WO_6 suspension, Bi_2WO_6 nanoparticles aggregate around TiO_2-NTs. Subsequently, at high temperature and high pressure, Bi_2WO_6 nanoparticles grow into curled flakes or smaller nanoparticles and homogeneously dispersed on the surface of TiO_2 nanotubes *in-situ* growth process, resulting in the formation of Bi_2WO_6/TiO_2-NTs heterojunction[31].

$$Bi(NO_3)_3+H_2O \xrightarrow{\text{Hydrolysis and condensation}} BiO(NO_3)+2H^++2NO_3^- \quad (\mathbf{1})$$

$$2BiO(NO_3)+H_2O \xrightarrow{\text{Hydrolysis and condensation}} Bi_2O_2(OH)(NO_3)+H^++NO_3^- \quad (\mathbf{2})$$

$$Bi_2O_2(OH)(NO_3)+WO_4^{2-}+H^+ \rightarrow Bi_2WO_6+NO_3^-+H_2O \quad (\mathbf{3})$$

2.3 Optical property

UV-Vis diffused absorption spectra (UV-Vis DRS) were carried out to investigate the optical properties of the photocatalysts. As shown in Fig.5a, the pure TiO_2-NTs and Bi_2WO_6 exhibit a fundamental absorption edge at around 388 and 450 nm, which originate from the charge transfer response of TiO_2-NTs and Bi_2WO_6 from the valence band to the conduction band, respectively[39]. Compared with pure TiO_2-NTs, the absorption edges of Bi_2WO_6/TiO_2-NTs showed obvious red-shift to the longer wavelength within the range of visible light.

It is known that the optical absorption near the band edge of prepared samples obeys the following equation: $(\alpha h\nu)^n=K(h\nu-E_g)$. In this equation, K, α, h, $h\nu$, E_g are constant, absorption coefficient, Planck constant, energy of the incident photon, band gap, respectively, and n is 0.5 and 1 for a direct and indirect band gap semi-conductor[38]. According to the formula, the calculated band gaps (E_g) of samples are 2.75 eV (Bi_2WO_6), 2.87 eV (Bi_2WO_6/TiO_2-NTs-25), 2.94 eV (Bi_2WO_6/TiO_2-NTs-35), 3.00 eV (Bi_2WO_6/TiO_2-NTs-50), and 3.20 eV (TiO_2-NTs), respectively.

The conduction band (CB) and valence band (VB) positions of the Bi_2WO_6 and TiO_2 samples are estimated by the following equations: $E_{VB}=X-E_e+0.5E_g$;

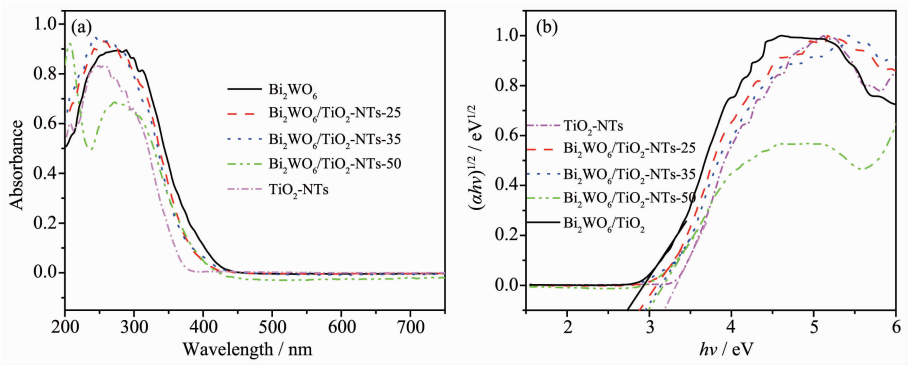

Fig.5 UV-Vis DRS (a) and plot of $(\alpha h\nu)^{1/2}$ versus $h\nu$ (b) for Bi_2WO_6, TiO_2-NTs and the Bi_2WO_6/TiO_2-NTs materials

$E_{CB}=E_{VB}-E_g$, where E_{VB} and E_{CB} are the VB and CB edge potentials, E_e is the energy of free electrons on the hydrogen scale (about 4.5 eV vs NHE). The X values for the Bi_2WO_6 and TiO_2 materials are 6.21 and 5.81 eV, respectively[40-41]. The E_g of Bi_2WO_6 and TiO_2-NTs are estimated to be 2.75 and 3.20 eV, respectively. Herein, the CB and VB edge potentials of Bi_2WO_6 and TiO_2-NTs are calculated at 0.34 and 3.09 eV, and −0.29 and 2.91 eV, respectively.

2.4 Photocatalytic activity

The photocatalytic performance of the Bi_2WO_6/TiO_2-NTs heterostructures in terms of photodegradation of RhB molecules under multiple modes including UV, visible, and microwave-assisted photocatalysis was investigated.

Fig.6a shows the photocatalytic activities of photocatalysts. Under UV light irradiation alone (without catalyst), only 3% RhB is degraded, which means the RhB can remain stability under long time irradiation. However, apparent changes in the concentration of RhB are observed in the existence of both light and catalyst. After irradiation for 90 min, 46.8%, 61.5%, 70.0%, 88.9%, 82.4% and 74.1% of the RhB is degraded by using the TiO_2-NTs, Bi_2WO_6, $Bi_2WO_6/$

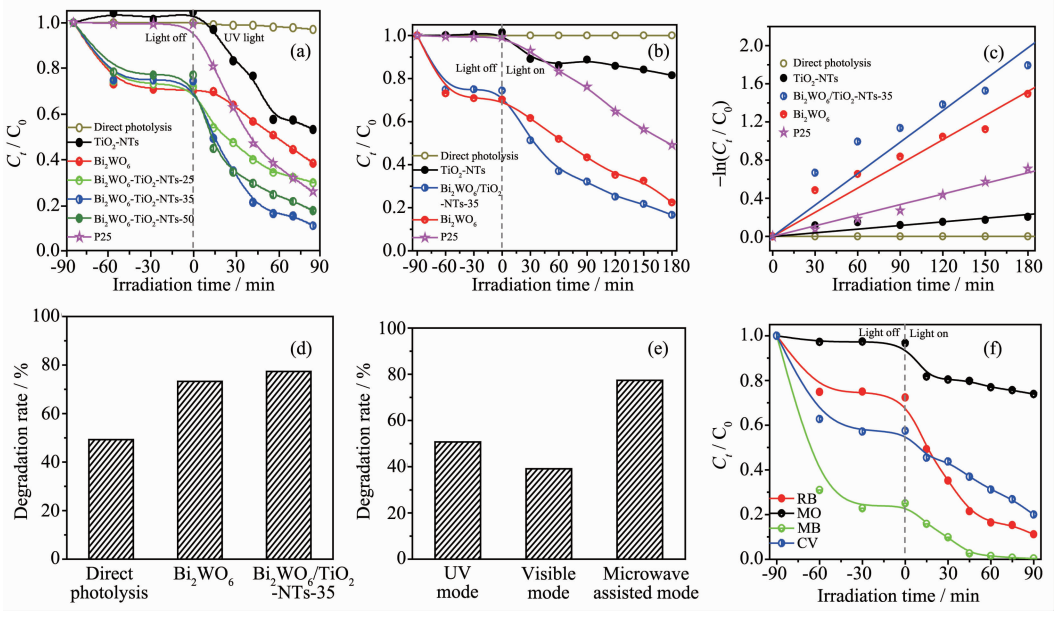

Fig.6 Normalized decrease concentration of C_t/C_0 of RhB solution containing different photocatalysts under UV (a) and visible (b) light irradiation; (c) $-\ln(C_t/C_0)$ as a function of irradiation time for RhB degradation over photocatalysts; (d) Photocatalytic degradation RhB profiles obtained using different photocatalysts under microwave-assisted photocatalysis mode for 15 min; (e) Photocatalytic degradation RhB profiles by Bi_2WO_6/TiO_2-NTs-35 obtained under multimode for 15 min; (f) Normalized decrease concentrations of C_t/C_0 of different dyes using Bi_2WO_6/TiO_2-NTs-35 under UV light irradiation

TiO_2-NTs-25, Bi_2WO_6/TiO_2-NTs-35, Bi_2WO_6/TiO_2-NTs-50, and P25, respectively.

Fig.6b displays the photocatalytic activity of prepared samples under the visible light irradiation. It is found that the photocatalytic performance of Bi_2WO_6/TiO_2-NTs-35 to degrade RhB under visible light irradiation surpasses that of its individual counterparts.

At the same time, the kinetics of photocatalytic degradation of RhB is investigated by simplified Langmuir-Hinshelwood model. The pseudo-first-order rate constant (k_{app}) is calculated using the formula $-\ln(C_t/C_0)=k_{app}t$, where C_0 and C_t are the initial concentration and concentration at reaction time t of RhB, respectively. From Fig.6c, under visible irradiation, the rate constant over Bi_2WO_6/TiO_2-NTs-35, Bi_2WO_6, P25, and TiO_2-NTs is 1.10×10^{-2}, 8.45×10^{-3}, 3.71×10^{-3}, and 1.27×10^{-3} min^{-1}, respectively. Moreover, Bi_2WO_6/TiO_2-NTs-35 shows the highest first-order rate constant, which is about 1.2 and 8.7 times greater than that of pure Bi_2WO_6 and TiO_2-NTs, respectively.

Fig.6d also exhibits the photocatalytic activity of different photocatalysts under microwave-assisted photocatalysis mode with electrodeless discharge lamp activated by microwaves as the light source. Bi_2WO_6/TiO_2-NTs-35 shows highest photocatalytic activity towards RhB degradation under microwave-assisted photocatalysis mode. Moreover, Fig.6e displays photocatalytic activities of Bi_2WO_6/TiO_2-NTs-35 under different modes after irradiation for 15 min. In contrast with UV and visible mode, the Bi_2WO_6/TiO_2-NTs-35 shows higher activity under microwave-assisted photocatalytic mode. In addition, different kinds of dyes were selected to evaluate the photocatalytic activity under UV light irradiation (Fig.6f). The cationic dyes (CV, MB, and RhB) are effectively degraded, while the degradation of anionic dye (MO) is poor, which is attributed to the different structure and adsorption of dyes.

To evaluate the stability and reusability of Bi_2WO_6/TiO_2-NTs-35 heterostructures for practical application, the photocatalytic degradation of RhB with the same photocatalyst is carried out for several times. As displayed in Fig.7, degradation curve has no obvious decline after four cycles of RhB degradation reaction under UV light irradiation, which indicates Bi_2WO_6/TiO_2-NTs-35 heterostructures maintain high stability.

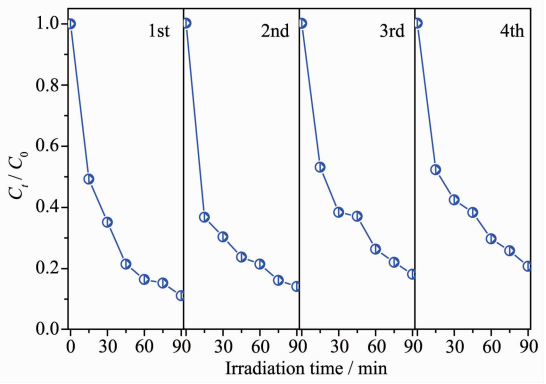

Fig.7　Recycling for the photodegradation of RhB in the presence of Bi_2WO_6/TiO_2-NTs-35 under UV light irradiation

2.5　Possible pathway of RhB degradation in Bi_2WO_6/TiO_2-NTs system

The above photocatalytic tests indicate that: (i) the photocatalytic activity of pure TiO_2-NTs can be further increased by introduction proper Bi_2WO_6 loading under multimode; (ii) in contrast to UV and visible mode, Bi_2WO_6/TiO_2-NTs showed higher photocatalytic activity under microwave-assisted photocatalysis mode. The influence factors towards the excellent photocatalytic activity of Bi_2WO_6/TiO_2-NTs are discussed.

Firstly, Bi_2WO_6 modified TiO_2 nanotubes play a major role in improving the photocatalytic activity of TiO_2 nanotubes. On one hand, according to UV-Vis DRS analysis, Bi_2WO_6/TiO_2-NTs heterostructures have a narrow band gap and exhibit enhanced UV and visible light absorption, consequently increases the utilization of light. On the other hand, the formed heterostructures between Bi_2WO_6 and TiO_2-NTs photocatalysts can extend the lifetime of photoinduced electrons and holes via an internal charge transfer, further facilitate the separation of e^--h^+ pairs and reduce the chance of recombination. These well-separated electrons and holes can participate in the overall photocatalysis process.

Secondly, the open mesoporous morphology of nanotubes can enhance the contact between the substance and photocatalysts during the photocatalytic reaction. Meanwhile, the nanotubes provide an efficient transport channel for photogenerated electrons.

Thirdly, degradation mode influences the photocatalytic activity of Bi_2WO_6/TiO_2-NTs heterostructures. Compared with UV and visible mode, Bi_2WO_6/TiO_2-NTs heterostructures display highest photocatalytic activity under microwave-assisted photocatalysis mode. Microwave enhances the reactants mobility and diffusion leading to increased exchange of reactants between catalyst surface and solution[42]. Moreover, more ·OH and $\cdot O_2^-$ radicals are generated by photocatalysis with microwave irradiation than photocatalysis alone to enhance the separation of e^--h^+ pairs[43-45], which will be confirmed by the following trapping experiments.

As shown in Fig.8, the RhB degradation rate under UV degraded mode decreases obviously with the addition of disodium ethylenediaminetetraacetate (EDTA-2Na, 1 mmol·L^{-1}) as scavenger for h^+ (from 88.9% to 9.3%), is moderately reduced with the addition of benzoquinone (BQ, 1 mmol·L^{-1}) as scavenger for $\cdot O_2^-$ (from 88.9% to 58.6%) and *tert*-butyl alcohol (*t*-BuOH, 1 mmol·L^{-1}) as scavenger for ·OH (from 88.9% to 73.7%)[46-48]. Similar results are found in RhB photodegradation over Bi_2WO_6/TiO_2-NTs-35 under visible mode. Compared with UV and visible mode, under microwave-assisted mode, there is a little difference. The degradation rate toward RhB exhibits a significant decrease when EDTA-2Na, BQ, and *t*-BuOH are introduced. Furthermore, RhB degradation rate is reduced from the original 77.4% to 23.9%, 30.7%, and 37.5%, respectively. These results suggest that: (i) under the three modes, the degradation of RhB is primarily driven by h^+, ·OH, and $\cdot O_2^-$; (ii) under the UV and visible mode, h^+ is the dominant reactive oxidants; (iii) under microwave-assisted mode, h^+, ·OH and $\cdot O_2^-$ make nearly equal contribution to RhB degradation. That is to say, more ·OH and $\cdot O_2^-$ are generated under microwave-assisted photocatalysis mode compared with UV and visible mode.

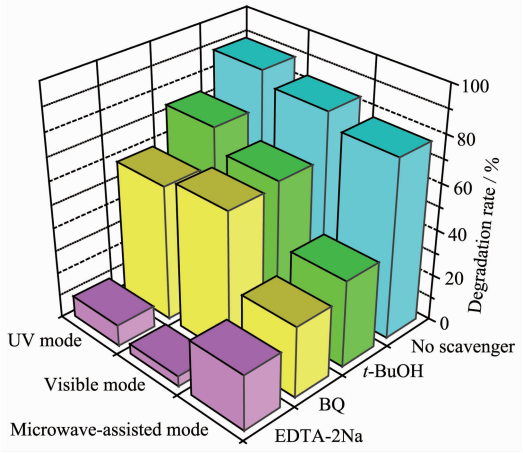

Fig.8 Controlled experiments using different radical scavengers for the degradation of RhB by Bi_2WO_6/TiO_2-NTs-35 under different modes

Based on the above results, the photocatalytic mechanism for Bi_2WO_6/TiO_2-NTs heterostructures photocatalyst is tentatively proposed and schematically illustrated in Scheme 1. The conduction bands (CB) (the valence band (VB), band gap) of TiO_2-NTs and Bi_2WO_6 are at −0.29 and 0.34 eV, respectively. Hence, under UV or MEL irradiation, both TiO_2-NTs and Bi_2WO_6 are excited, and photogenerated electrons and holes are in their CB and VB, respectively. Subsequently, the photoexcited electrons in the CB of TiO_2-NTs transfer to the CB of Bi_2WO_6, which is due to that E_{CB} of TiO_2-NTs is more negative than that of Bi_2WO_6. Simultaneously, the holes in the E_{VB} of Bi_2WO_6 move to TiO_2-NTs due to that the E_{VB} of Bi_2WO_6 is more positive than that of TiO_2-NTs. The h_{VB}^+ reacts with the absorbed H_2O molecules or deoxidizes dioxygen dissolved in the aqueous solution to form ·OH radicals. In addition, the E_{CB} can be easily oxidized by dioxygen to produce $\cdot O_2^-$ radicals. With the help of ·

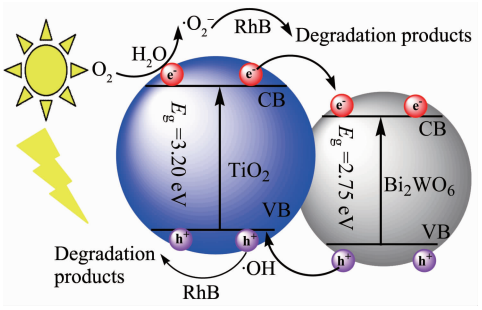

Scheme 1 Photodegradation mechanism of Bi_2WO_6/TiO_2-NTs-35 heterostructures photocatalyst under UV mode

OH, h_{VB}^+ and $\cdot O_2^-$ species, RhB is degraded and then mineralized. The photocatalytic process under visible light irradiation is similar with UV (microwave-assisted photocatalytic mode) except TiO_2-NTs are not excited.

3 Conclusions

In summary, Bi_2WO_6/TiO_2-NTs heterostructures were fabricated by multicomponent assembly approach combined with hydrothermal treatment. Bi_2WO_6 flakes or nanoparticles dispersed on the surface of TiO_2 nanotubes to form heterostructures. The prepared Bi_2WO_6/TiO_2-NTs heterostructures exhibit considerably high photocatalytic activity towards the degradation of RhB under multimode including UV, visible and microwave-assisted photocatalysis. This enhanced photocatalytic activity is due to more efficient separation of the e^--h^+ pairs, originating from the introduction of Bi_2WO_6 modified TiO_2-NTs, the nanotubular geometries, and the degradation mode. The h^+, $\cdot OH$, and $\cdot O_2^-$ radicals are the main active species during the photocatalysis process under multimode. Moreover, more $\cdot OH$ and $\cdot O_2^-$ radicals are generated by photocatalyst with microwave-assisted irradiation. This work can provide important inspirations in developing the photocatalytic heterostructures materials.

Acknowledgments: This work is supported by the Natural Science Foundation of China (Grants No.21376126, 81403067), the Program for Young Teachers Scientific Research in Qiqihar University (Grant No.2014K-M03), and the Basic Business Special Scientific Research of Heilongjiang Province Education Department (Grant No.135109204).

References:

[1] Tian J, Zhao Z H, Kumar A, et al. *Chem. Soc. Rev.*, **2014**, **43**:6920-6937

[2] Daghrir R, Drogui P, Robert D. *Ind. Eng. Chem. Res.*, **2013**, **52**:3581-3599

[3] Sang L X, Zhao Y X, Burda C. *Chem. Rev.*, **2014**,**114**:9283-9318

[4] ZHANG Chao-Ying(张超颖), WANG Ping(王苹), LIU Yan-Yan(刘岩岩), et al. *Chinese J. Inorg. Chem.*(无机化学学报), **2017**,**33**(7):1132-1138

[5] Murciano L T, Lapkin A A, Chadwick D. *J. Mater. Chem.*, **2010**,**20**:6484-6489

[6] Zhang Y L, Han C, Zhang G S, et al. *Chem. Eng. J.*, **2015**, **268**:170-179

[7] Lee K, Mazare A, Schmuki P. *Chem. Rev.*, **2014**,**114**:9385-9454

[8] Wang X D, Li Z D, Shi J, et al. *Chem. Rev.*, **2014**,**114**:9346-9384

[9] Wehrenfennig C, Palumbiny C M, Snaith H J, et al. *J. Phys. Chem. C*, **2015**,**119**:9159-9168

[10]Wang H L, Zhang L S, Chen Z G, et al. *Chem. Soc. Rev.*, **2014**,**43**:5234-5244

[11]Li J, Fang W, Yu C L, et al. *Appl. Surf. Sci.*, **2015**,**358**:46-56

[12]Yu C L, Zhou W Q, Yu J C, et al. *Chin. J. Catal.*, **2014**,**35**:1609-1618

[13]Yu C L, Wei L F, Chen J C, et al. *Ind. Eng. Chem. Res.*, **2014**,**53**:5759-5766

[14]Yu C L, Li G, Kumar S, et al. *Adv. Mater.*, **2014**,**26**:892-898

[15]Yu C L, Wei L F, Zhou W Q, et al. *Chemosphere*, **2016**, **157**:250-261

[16]Yu C L, Zhou W Q, Liu H, et al. *Chem. Eng. J.*, **2016**,**287**:117-129

[17]Yu C L, Zhou W Q, Zhu L H, et al. *Appl. Catal. B*, **2016**, **184**:1-11

[18]Yu C L, Wu Z, Liu R Y, et al. *Appl. Catal. B*, **2017**,**209**:1-11

[19]Zhang J, Xu Q, Feng Z C, et al. *Angew. Chem. Int. Ed.*, **2008**,**47**:1766-1769

[20]Zong X, Yan H J, Wu G P, et al. *J. Am. Chem. Soc.*, **2008**, **130**:7176-7177

[21]Zhang F, Zhang C L, Peng H Y, et al. *Part. Part. Syst. Char.*, **2016**,**33**:248-253

[22]Zhang F, Zhang C L, Wang W N, et al. *ChemSusChem*, **2016**,**9**:1449-1454

[23]Xu Z H, Quintanilla M, Vetrone F, et al. *Adv. Funct. Mater.*, **2015**,**25**:2950-2960

[24]Zhou F Q, Fan J C, Xu Q J, et al. *Appl. Catal. B*, **2017**,**201**:77-83

[25]Zhang F, Wang W N, Cong H P, et al. *Part. Part. Syst. Char.*, **2017**,**34**(2):1600222(6 pages)

[26]Min Y L, He G Q, Xu Q J, et al. *J. Mater. Chem. A*, **2014**, **2**:2578-2584

[27]Zhang L S, Wang H L, Chen Z G, et al. *Appl. Catal. B*, **2011**,**106**:1-13

[28]ZHANG Tian(张田), ZOU Zheng-Guang(邹正光), HE Jin-Yun(何金云), et al. *Chinese J. Inorg. Chem.*(无机化学学报), **2017**,**33**(6):954-962

[29]Huang J, Tan G Q, Ren H J, et al. *ACS Appl. Mater.*

Interfaces, **2014**,**6**:21041-21050

[30]Zhang L W, Zhu Y F. *Catal. Sci. Technol.*, **2012**,**2**:694-706

[31]Zhang Y P, Fei L F, Jiang X D, et al. *J. Am. Ceram. Soc.*, **2011**,**94**:4157-4161

[32]López S M, Hidalgo M C, Navío J A, et al. *J. Hazard. Mater.*, **2011**,**185**:1425-1434

[33]Liu Z, Liu X Z, Lu D Z, et al. *Mater. Lett.*, **2014**,**130**:143-145

[34]Hou Y F, Liu S J, Zhang J H, et al. *Dalton Trans.*, **2014**,**43**:1025-1031

[35]Li Y, Wu W J, Wu M Z, et al. *Mater. Res. Bull.*, **2014**,**55**:121-125

[36]Deng F, Liu Y, Luo X B, et al. *Sep. Purif. Technol.*, **2013**, **120**:156-161

[37]Ma F Y, Geng Z, Yang X, et al. *RSC Adv.*, **2015**,**5**:46677-46685

[38]Chen S F, Tang W M, Hu Y F, et al. *CrystEngComm*, **2013**, **15**:7943-7950

[39]Di J, Xia J X, Ge Y P, et al. *Appl. Catal. B*, **2015**,**168-169**:51-61

[40]Li L, Huang X D, Hu T Y, et al. *New J. Chem.*, **2014**,**38**:5293-5302

[41]Dai K, Lu L H, Liang C H, et al. *Appl. Catal. B*, **2014**,**156-157**:331-340

[42]Zhang X W, Li G T, Wang Y Z. *Dyes Pigm.*, **2007**,**74**:536-544

[43]Genuino H C, Hamal D B, Fu Y J, et al. *J. Phys. Chem. C*, **2012**,**116**:14040-14051

[44]Zhang Z H, Yu F Y, Huang L R, et al. *J. Hazard. Mater.*, **2014**,278:152-157

[45]Zhang X W, Sun D D, Li G T, et al. *J. Photochem. Photobiol. A*, **2008**,**199**:311-315

[46]Xiao J D, Xie Y B, Cao H B, et al. *Catal. Commun.*, **2015**, **66**:10-14

[47]Lin S L, Liu L, Hu J S, et al. *Appl. Surf. Sci.*, **2015**,**324**:20-29

[48]Ma F Y, Shi T, Gao J, et al. *Colloids Surf. A*, **2012**,**401**:116-125